NUMERICAL MODELING OF DEBRIS IMPACTS USING THE SPH METHOD

Steffanie Piche[1], Ioan Nistor[2], and Tad Murty[3]

The significance of coastal forests as a protection barrier against tsunami waves has been of particular interest following recent tsunami events. Coastal forests have been shown to attenuate tsunami–induced inundation and are believed to be capable of reducing the propagation of tsunami-borne debris onshore. The current paper aims to examine the suitability of using a Smoothed Particle Hydrodynamics (SPH) model to (1) simulate debris impact forces acting on a structure and (2) to determine if it is possible for a small coastal forest to attenuate tsunami-borne debris. The results of this study indicate that the SPH model utilized was able to reasonably replicate the hydrodynamic forces acting on structures and the water surface elevation, but was not able to reproduce the large debris impact forces observed in an experimental test program. However, the authors concluded that coastal forests can potentially provide protection against floating debris.

Keywords: SPH; debris impacts; coastal forests

INTRODUCTION

Damage caused by large tsunami events such as the 2011 Tohoku Tsunami resulted in billions of dollars in economic losses and claimed more than 250,000 lives during the past ten years alone. These extreme events can result in significant damage to the infrastructure of coastal communities through both the tsunami inundation itself and the large volume of debris that is generated and propagates inland with the tsunami-induced flow.

Methods of protecting communities include man-made measures such as massive seawalls and breakwaters, which are designed to prevent the inland propagation of the tsunami bore. Other protection methods are in the form of natural barriers, such as coastal forests which can attenuate the tsunami as it travels inland. While such barriers have been shown in previous studies to be capable of attenuating the impact of tsunami inundation, there is also a risk that the entire forest or a portion of it may fail, generating itself a large volume of woody debris. In the case of no failure or a partial failure it is necessary to determine whether the coastal forest is also capable of attenuating tsunami-borne debris, preventing them from traveling inland and affecting local communities.

The ability of the coastal forest to attenuate debris requires an in-depth understanding of the debris impact forces that can be generated by tsunami-borne debris. These forces are highly dependent on a number of parameters which can make them difficult to estimate analytically. FEMA P-55 [2011] indicates that the debris impact force is reliant on the size, shape and mass of the debris itself which can be predicted through site-specific studies, and also on the velocity, duration of the impact, impact angle, building type and location of the impact relative to the building geometry, all elements which are difficult to predict. As such, it can be extremely difficult to get accurate estimates of the impact forces which may act on a structure during a tsunami event.

The current study focuses on the ability of the SPH model DualSPHysics V2.0 in reproducing the propagation and impact force of wooden debris on a cylindrical structure based on the experimental work performed by Al-Faesly *et al.* [2013], and applying the method to a larger scale model of a small coastal forest. The objective of this research was to determine if the model could correctly replicate the debris propagation and subsequent impact on the structure and the debris impact forces when compared to those obtained in the physical model. The secondary objectives of the study were to investigate whether coastal forest could be used to attenuate the propagation of tsunami-borne debris, and to compare the results of the physical and numerical results with those provided by the FEMA P-646 [2012] and FEMA P-55 [2011]design guidelines.

CURRENT DESIGN GUIDELINES

This study compares the numerically calculated and experimentally-recorded impact forces with two FEMA design guidelines (FEMA P-55 [2011] and FEMA P-646 [2012]) which are currently in use to assess the different impact forces caused by a tsunami event, such as the hydrodynamic force and the debris impact force. The impact forces calculated using these guidelines are compared with the results from the physical experiment and those obtained using the numerical model in a subsequent section.

The FEMA P-55 guideline [2011] is based on the premise that the magnitude of the debris impact force on a structure is dependent on the flow conditions surrounding the building as well as on the

[1]Graduate Student, Department of Civil Engineering, University of Ottawa, Ottawa, Ontario, Canada
[2]Associate Professor, Department of Civil Engineering, University of Ottawa, Ottawa, Ontario, Canada
[3] Adjunct Professor, Department of Civil Engineering, University of Ottawa, Ottawa, Ontario, Canada

characteristics of the debris. The guideline suggests the following equation for the prediction of the debris impact force:

$$F_i = WVC_D C_B C_{Str} \tag{1}$$

where F_i is the debris impact force, W is the weight of the debris, and V is the velocity of the water, which is assumed to be moving at the same velocity as the debris. Coefficients C_D, C_B, and C_{Str} are the coefficients of depth, blockage and building structure, respectively. The depth coefficient is intended to account for any reductions in the debris velocity due to decreased water depth when it approaches the impacted structure: its value can vary from 0.0 for stillwater floods of depths greater or equal to 1ft, to up to 1.0 for floods with depths greater than or equal to 5ft. The blockage coefficient, C_B, accounts for any upstream screening which may result in a reduction in the debris velocity. The value of this coefficient ranges from 0.0 for areas with dense screening to 1.0 for areas with no upstream screening. Coefficient, C_{str}, is used to represent the type of structure being impacted. A value of 0.2 can be used for a timber pile or masonry supported structure, 0.4 for concrete piles or moment resistant frames and 0.8 for reinforced concrete foundation walls. This value can also be determined analytically for structures not listed, depending on the duration of impact and the importance of the impacted structure.

The 2012 FEMA P-646 guideline proposed a new debris impact force equation when compared to previous editions of the guideline. The new recommended equation is:

$$F_i = 1.3u_{max}\sqrt{km_d(1+c)} \tag{2}$$

where the debris impact force is dependent on the maximum flow velocity, u_{max}, the debris mass, m, and the effective net combined stiffness of the debris and the impacted structure, k. The hydrodynamic mass coefficient, c, is used to represent the effect of the flow movement on the debris, with typical values ranging from 0.0 to 1.0 depending on the debris mass and its orientation relative to the flow direction. The constant 1.3 represents the importance coefficient for buildings in the risk category IV, as specified in ASCE 7 [2010] for debris impacts.

SPH MODEL

The Smoothed Particle Hydrodynamics (SPH) method is a Lagrangian-based mesh-free method introduced in 1977 by Gingold and Monaghan, and Lucy for use in modeling astrophysical and cosmological phenomena. In 1994 Monaghan adapted this method for use in fluid dynamics and now this method has applications in both computational solid mechanics and computational fluid mechanics where it has been used to study free surface waves [Monaghan and Kos, 1999], wave breaking and wave impacts [Lo and Shao, 2002]. The benefits of this mesh-frees model over a meshed model are that it allows for complex geometries to be modeled easily and is able to reproduce large surface deformations. The model selected for this study was DualSPHysics [Crespo *et al.*, 2011; Gómez-Gesteira *et al.*, 2010, 2012a, 2012b] which is able to run on the computers graphics processing unit (GPU) resulting in a decreased computational effort. Comprehensive analyses of the SPH method can be found in Liu and Liu [2003], Monaghan [2005] and St-Germain [2012].

The main principle behind the SPH method is that it represents the physical domain as a set of arbitrarily distributed particles which each possess individual properties, such as mass, velocity and position. These properties are approximated for an individual particle, i, using a functional approximation:

$$f(\boldsymbol{x}_i) = \sum_{j=1}^{N} \frac{m_j}{\rho_j} f(\boldsymbol{x}_i) W_{ij} \tag{3}$$

where $\boldsymbol{x}_i$ is the position vector of the particle of interest, i, and m_j and ρ_j are the masses and density of the neighboring particles j, respectively. N is the number of particles within the domain of influence that contribute to the function approximation. The smoothing kernel, W_{ij}, also known as the weighting function, is described as follows:

$$W_{ij} = W(x_i - x_j, h) \tag{4}$$

where the smoothing length, h, is used to control the size of the influence domain, Ω around the particle of interest, see example in Figure 1.

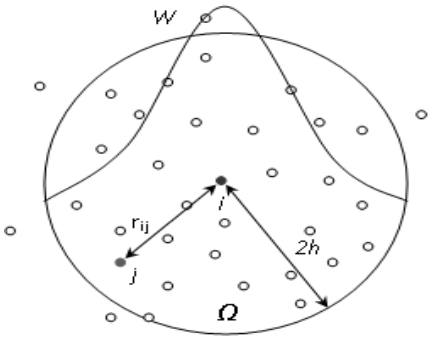

Figure 1. Domain of influence around particle i for a smoothing function, W, of radius 2h.

The smoothing kernel, *W,* selected for use in the current study was the cubic spline kernel which is represented by the relationship:

$$W_{ij} = \alpha_D \begin{cases} 1 - \frac{3}{2}q^2 + \frac{3}{4}q^3 & 0 \le q \le 1 \\ \frac{1}{4}(q)^3 & 1 \le q \le 2 \\ 0 & q \ge 2 \end{cases} \quad (5)$$

where $q = r_{ij}/h$ and $\alpha_D = 5/(\pi 4h^3)$ for three-dimensional space.

Governing Equations

The physical conservation laws of momentum and continuity are implemented in the SPH method as the compressible Navier-Stokes equations in Lagrangian form. These equations are, respectively:

$$\frac{Du}{Dt} = -\frac{1}{\rho}\nabla P + g + DiffusionTerms \quad (6)$$

$$\frac{1}{\rho}\frac{D\rho}{Dt} = -\nabla \cdot u \quad (7)$$

where $D\boldsymbol{u}/Dt$ is the derivative of the fluid velocity, $\boldsymbol{u}$, with respect to time and $D\rho/Dt$ is the derivative of the fluid density, ρ, with respect to time. Benz [1990] suggested an approach in which the equations could be discretized into ordinary differential equations which can be resolved through integration by time. Based on this method, equations 6 and 7 can be rewritten as:

$$\frac{Du_i}{Dt} = -\sum_{j=1}^{N} m_j \left(\frac{P_i + P_j}{\rho_i \rho_j}\right) \nabla_i W_{ij} + g + DiffusionTerms \quad (8)$$

$$\frac{D\rho_i}{Dt} = \sum_{j=1}^{N} \frac{m_j}{\rho_j}\left(u_i - u_j\right) \cdot \nabla_j W_{ij} \quad (9)$$

where $\boldsymbol{u_i}$, $\boldsymbol{u_j}$, P_i and P_j are the velocity vectors and pressures for the particles i and j, respectively.

The pressure term shown in equation 8, is calculated using an equation of state. The use of this equation indicates that the fluid is treated as weakly compressible, which is less computationally intensive then treating it as incompressible liquid. The equation of state was developed by Batchelor [1974] and was then modified by Monaghan [1994]:

$$P_i = \frac{c_0^2 \rho_0}{\gamma}\left[\left(\frac{\rho_i}{\rho_0}\right)^{\gamma} - 1\right] \tag{10}$$

where γ is equal to 7, ρ_0 is the reference water density (equal to 1000 kg/m^3), and c_0 is the speed of sound in the water for the reference density. For the assumption of weakly compressible flow to be valid, the density variation in the fluid is required to remain within a 1% range.

Time Integration

The current study used the Verlet time integration algorithm [Verlet, 1967]. This time integration scheme is commonly used and is based on the third-order Taylor expansion for the momentum, density, position and density of energy of the particles.

The SPH model time step is controlled by the Courant-Fredrich-Levy condition (CFL condition), the viscous diffusion in the fluid [Monaghan, 1989] and the magnitude of the external and internal forces that act on the fluid particles:

$$\Delta t = \propto_{time} min_i\left(\Delta t_f, \Delta t_{CV}\right) \tag{11}$$

where the time step required by the internal and external force condition is represented by Δt_f, and Δt_{CV} is the time step required by the combined CFL and viscosity conditions. The constant α_{time} is typically selected as 0.3 but can range from 0.1 to 0.5.

Viscosity

Artificial viscosity was implemented as the model used did not have any additional options for use with floating objects. Artificial viscosity is not designed to represent actual viscosity but is designed to allow for shock phenomena to be modeled, resulting in a more stable model. Artificial viscosity is implemented by rewriting the momentum equation (Equation 8) as:

$$\frac{D\boldsymbol{u}_i}{Dt} = -\sum_j m_j\left(\frac{P_i}{\rho_i^2} + \frac{P_j}{\rho_j^2} + \Pi_{ij}\right)\nabla_i W_{ij} + \boldsymbol{g} \tag{12}$$

where the viscosity term, Π_{ij}, is given by:

$$\Pi_{ij} = \begin{cases} \frac{-\alpha_{visc} c_{ij}\mu_{ij} + \beta\mu_{ij}^2}{\rho_{ij}} & \boldsymbol{u}_{ij}\cdot\boldsymbol{x}_{ij} < 0; \\ 0 & \boldsymbol{u}_{ij}\cdot\boldsymbol{x}_{ij} > 0; \end{cases} \tag{13}$$

and,

$$\mu_{ij} = \frac{h\boldsymbol{u}_{ij}\cdot\boldsymbol{x}_{ij}}{\boldsymbol{x}_{ij}^2 + \eta^2} \tag{14}$$

When $\boldsymbol{u}_{ij}\cdot\boldsymbol{x}_{ij}$ is greater than zero, then there is no viscosity in the system, as shown in equation 13, while viscosity is present when $\boldsymbol{u}_{ij}\cdot\boldsymbol{x}_{ij}$ is less than zero. The constant α_{visc} is a user-defined parameter which is highly variable depending on the problem being examined, the constant β is typically in the order of $\eta^2 = 0.01h^2$.

Boundary Conditions

The current model only allowed one option for the treatment of the model boundary and solid objects, namely the dynamic boundary condition [Crespo *et al.*, 2007]. This boundary condition employs dynamic boundary particles which are governed by the same conservation equations as the fluid particles, with their properties being similarly calculated. However, unlike the fluid particles these particles have an imposed location or movement that they cannot deviate from, with the exception of floating bodies which are free to move around as a unit.

These boundary conditions are used to create repulsive forces which prevent the movement of the fluid particles through the floating bodies, domain walls or solid objects. In order for this to function, the dynamic boundary particles will repulse the incoming fluid particles through an increase in pressure. This increase in pressure results in a repulsive force which acts on the fluid particles and prevents them from breaching the dynamic boundaries. It should be noted that if the fluid particles have enough momentum then it is still possible for them to pass through the boundary layer.

In this study, three different boundary conditions were used for: (1)the outer domain walls and the impacted structures which used boundary particles with an imposed location; (2) the wavemaker which was used to generate a solitary wave based on a prescribed wave paddle motion; (3) the floating objects which used floating boundary particles that allowed for structures to be created that will respond and react according to the movement of the surrounding fluid and boundary particles.

EXPERIMENTAL SETUP

Two computational domains were used for this study: the first domain used was based off the experimental model by Al-Faesly *et al.* [2013] for the physical modeling of tsunami-borne debris impacts on near-shore cylindrical structures. The second domain used in this study was a larger scale model of a small stand of trees in order to determine how coastal forests may be able to attenuate the propagation of the tsunami-borne debris. This section covers details of the physical model as well as the computational domains and key parameters used for this study.

Physical Experiment

The physical experiments were performed by Al-Faesly *et al.*[2013] in a high-discharge flume located at the Ocean, Coastal and River Engineering Laboratory at the National Research Council (NRC) in Ottawa, Canada. This stainless steel flume has a total length of 14.56m, a width of 2.7m and a total depth of 1.4m. For this experiment, the flume was partitioned into two sections such that the reservoir could impound a larger volume of water despite the length restrictions of the flume. This also allowed for a longer bore impact on the downstream structure. The impounded water was released by use of a rapidly-opening swinging gate to allow the water to travel through a rectangular flume section which was 10.83m long and 1.3m wide. The bore was then evacuated at the downstream end of the flume using a floor drain that eliminated any impacts on the propagation of the bore (see Figures 2 and 3 for the model domain).

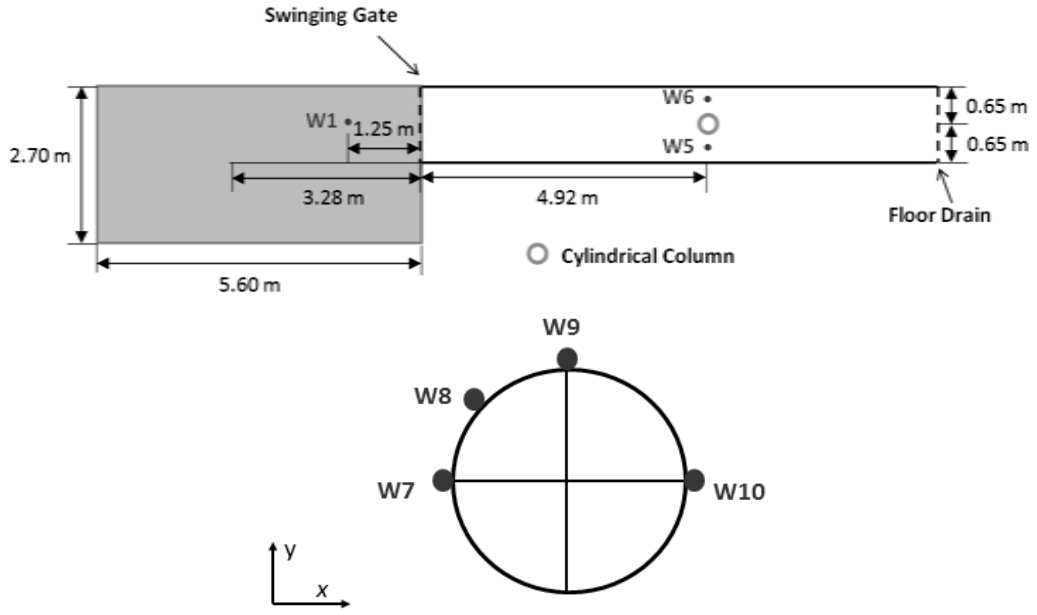

Figure 2. (a) Physical model domain and (b) cross-section of the column with the location of the gauges attached to its surface

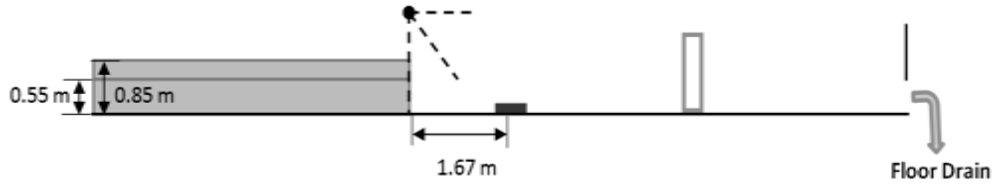

Figure 3. Side view of the physical model domain depicting the location of the debris and the reservoir impoundment depths

The swinging gate was sealed using water stops in order to prevent any water from leaking into the test flume; however, during testing, minor leakage was seen to occur due to the high impoundment depths tested. This resulted in the tests be performed under pseudo dry-bed conditions with downstream water depths of approximately 0.03m at certain locations. These water depths were not constant over the flume floor. A visual of the impounding reservoir and swinging gate can be seen in Figure 4.

Figure 4. Physical model impoundment reservoir and gate

Downstream of the gate, a hollow cylindrical acrylic structure was positioned along the centerline of the flume at a location of 4.92m downstream from the gate. The cylinder had an outside diameter of 0.305m and a height of 1m. It was fastened to the floor using a six-degree-of-freedom (6DOF) high frequency dynamometer which recorded the total base shear forces acting on the structure. The time-history of the water surface elevation was captured at seven locations in the flume using capacitance wave gauges as shown in Figure 2.

The physical experiments modeled the debris using wooden posts which were manufactured into different lengths and widths. The tested debris models, shown in Figure 5, had sizes of: 76.2mm x 76.2mm x 490mm, 76.2mm x 152.4mm x 490mm and 76.2mm x 76.2mm x 916mm,with masses of 1.088kg, 2.258kg, and 2.191kg, respectively. The debris was sealed with a waterproof coating in order to ensure that water intrusion would not alter the intended mass of the debris.

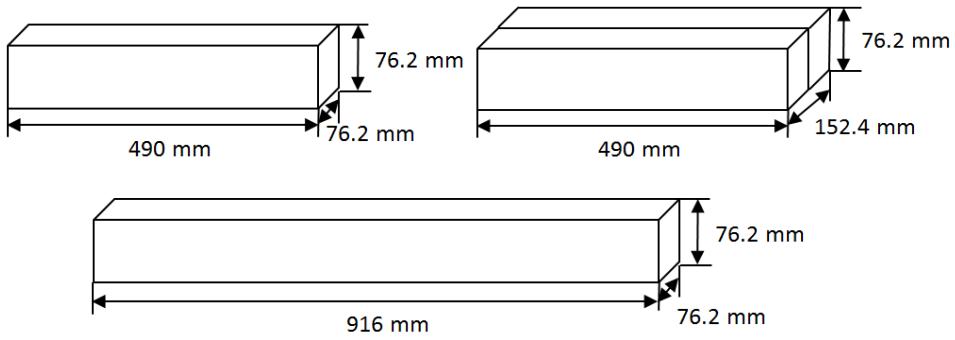

Figure 5. Debris models used for the physical and numerical models

Computational Setup

The computational setups of the numerical models are briefly outlined in this section. The domain used for the first set of numerical simulations was identical to that of the physical model, as shown in Figure 2, with the exception of an extension of the flume downstream of the cylindrical column. The purpose of this extension was to ensure that the floating debris remained inside the domain after the initial impact, as the computation would otherwise end prematurely. The full domain can be seen in Figure 6 for the initial setup of the model.

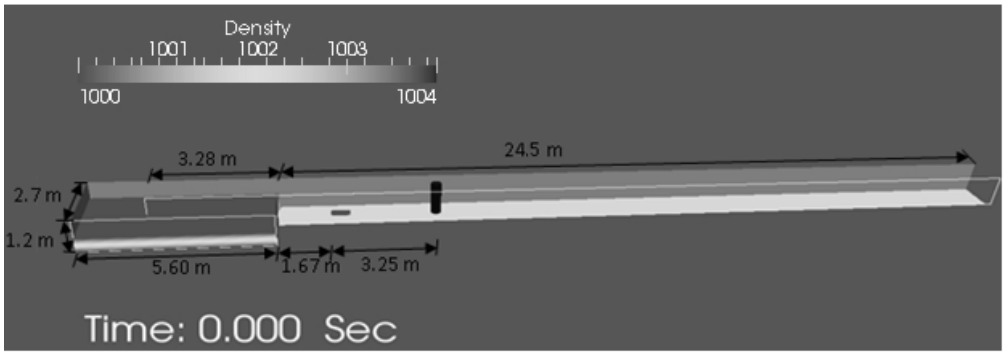

Figure 6. Computational domain of the numerical model

The results obtained from the model were the time-history of the water surface elevation at the seven gauges shown in Figure 2, the time-history of the hydrodynamic and bore impact force acting on the column, and the debris impact force acting in the model. This force was calculated based on the momentum-impulse principle.

The model used a uniform inter-particle spacing (Δ) of 0.025m in all direction, which resulted in a model smoothing length of 0.0375m. The tests using an impoundment depth of 0.55m employed a total of 998,574 fluid particles, while the larger impoundment depth of 0.85m had a total of 1,569,318 fluid particles. A list of the modeled scenarios is shown in Table 1. The simulations were completed using the DualSPHysics software [Crespo *et al.*, 2011; Gómez-Gesteira *et al.*, 2010, 2012a, 2012b], on GPU-equipped processors in order to decrease the computational cost of the numerical runs corresponding to a physical model time of 10s.

Table 1. Model test cases

Test Number	Impoundment Depth (m)	Debris Mass (kg)
1	0.55	1.088
2	0.55	2.258
3	0.55	2.191
4	0.85	1.088
5	0.85	2.258
6	0.85	2.191

The computational domain of the second simulation can be seen in Figure 7, this domain used a modeled wavemaker in order to generate a solitary wave. The debris modeled in this scenario had a diameter of 0.25m, as did the modeled trees, a length of 1.5m and a mass of 68kg. The group of tree used to represent a small patch of coastal forest used in the numerical model was located at a distance of 34m from the wavemaker with two rows of two trees spaced equally.

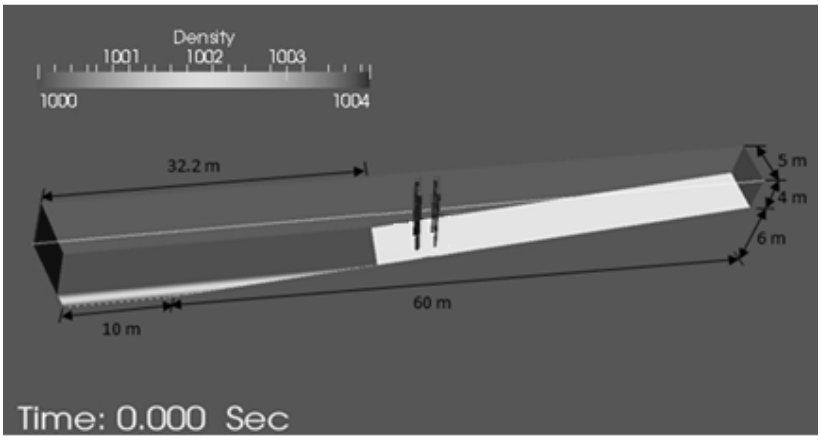

Figure 7. Computational domain of the coastal forest model

The results obtained from this model were the time-history of the hydrodynamic and bore impact forces acting on the individual trees, as well as the time-history of the debris impact forces on the trees. Similar to the bore model, the debris force was calculated based on the momentum-impulse principle.

Due to the size of the model, a uniform inter-particle spacing of 0.075m was used in all directions, resulting in a smoothing length of 0.1125m. The still-water level in the model was 2.25m, while the solitary wave generated by the wavemaker was 2.5m. The model had a total of 1,036,750 fluid particles and was run for a period of 25s. The same computational domain was used for four different initial debris locations.

RESULTS

This section presents results of the numerical model in comparison with those obtained from the physical experiments by Al-Faesly *et al*. Additional comparisons of the numerical and physical model with the FEMA P-55 [2011] and P-646 [2012] analytical results are included. The final results shown are those of the debris propagating through coastal forest model; however, no physical model comparisons were available for these tests. Only a selection of the results is shown.

Comparison of Numerical and Physical Model Results

Water Surface Elevation. The water surface elevation was obtained for both models at seven wave gauges located in the flume, as shown in Figure 2. The results of the numerical model were compared with those of the physical model at these gauges for four out of the six tests (results were not yet available for the last two tests). This comparison was intended to investigate if the numerical model could represent both the drawdown of the bore in the impounding reservoir and the water elevation on the structure (cylindrical column) during the initial impact and the subsequent sustained flow.

The results shown from this test are those of the 0.55m and 0.85m impoundment depths with the 1kg debris. From these comparisons it was determined that the initial drawdown in the reservoir was relatively good for both impoundment depths (Figure 8 (1) and 9 (1)), though there was a slight difference in the numerically and physically modeled results after the initial drawdown. The water surface elevation was reasonably well modeled along the sides of the column (Figures 8 (2) and (5) and Figures 9 (2) and (5). Unfortunately, the numerical model did show a large discrepancy for the gage located at the front of the column (Figure 8 (3) and (4) and Figure 9 (3) and (4)) as the numerical model was not able to capture the runup of the bore on the cylinder during impact. This lowered water surface elevation is believed to be caused by the presence of the debris in front of the structure during impact.

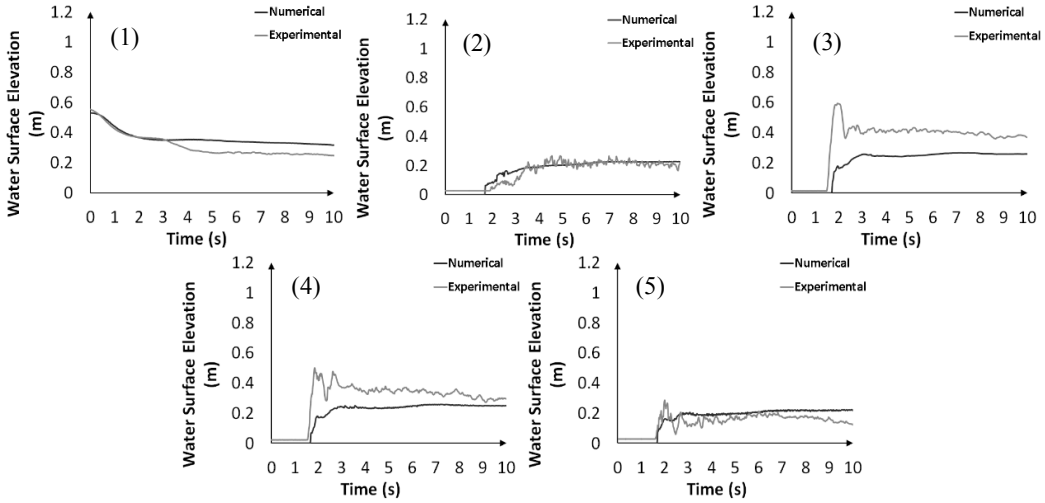

Figure 8.Time-history of the water surface elevation for an impoundment depth of 0.55m

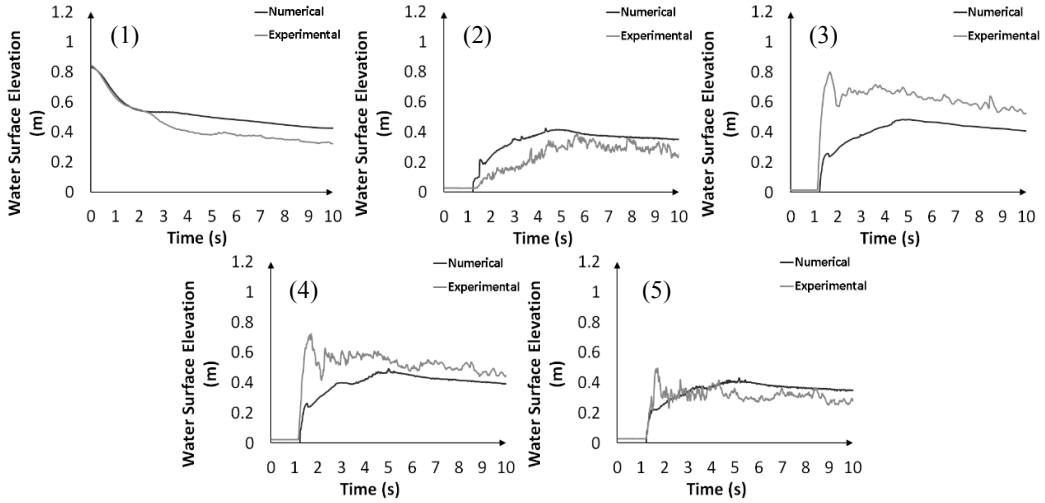

Figure 9.Time-history of the water surface elevation for an impoundment depth of 0.85m

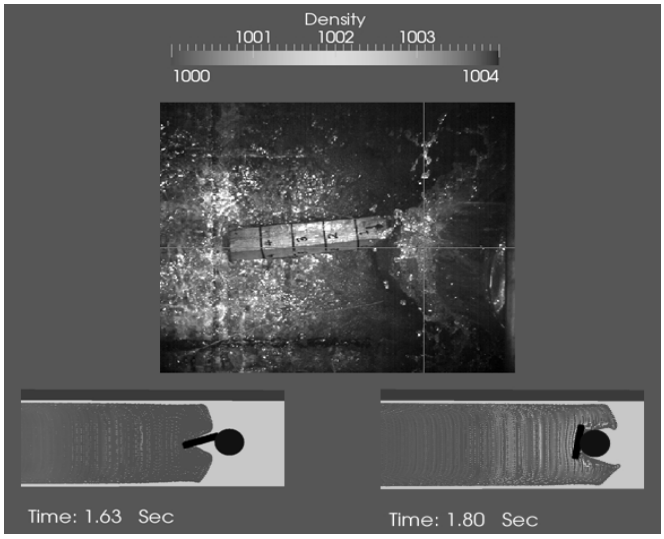

Figure 10. Numerical and physical model debris impacts for the 0.55m impoundment depth

Figures 10 and 11 show the debris impacts of both the physical and numerical results for the 0.55m and 0.85m impoundment depths. From these comparisons, one can notice that the debris impact location and angle were reasonably well modeled with the debris typically striking near the center of the column at roughly right angles. Slight variations did occur, as shown in Figure 11, where the debris impacted closer to the side of the column. The main difference between the impacts in the physical tests and numerical model was that the numerical debris was seen to rotate upon impact in many of the numerically runs, occasionally causing a secondary impact on the structure. This rotation caused the debris to block the front of the cylinder reducing the runup at impact.

A significant difference between the numerically and physically modeled debris was that the debris were generally propagating in front of the bore in the numerical model as opposed to on top of the bore as in the physical tests, resulting in it impacting the structure first. This did not occur in the physical model as the debris was physically picked up by the bore and impacted the structure at roughly the same time as the surrounding flow. A possible resolution for this error could be the use of a smaller inter-particle spacing which would allow the fluid particles to get closer to the debris without it moving – tests are currently underway.

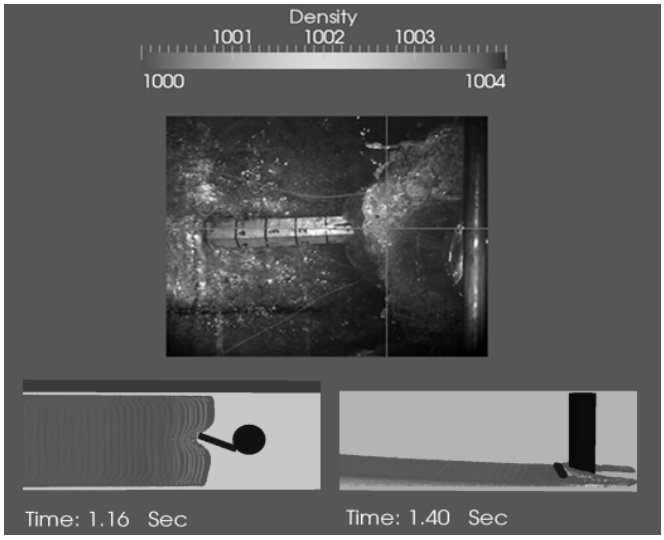

Figure 11. Numerical and physical model debris impacts for the 0.85m impoundment depth

Debris and Hydrodynamic Impact Forces. Due to the method used to obtain the impact forces of the debris and the bore on the structure, the numerically modeled debris and hydrodynamic forces were obtained separately and combined for comparison with the experimental results.

When comparing the combined hydrodynamic and debris numerical forces with those obtained from the physical model, for all model scenarios the numerical model was not able to accurately replicate the large peak impact forces on the structure, as shown in Figure 12 and 13. After the initial impact, the hydrodynamic force acting on the structure was found to be better modeled, especially for the larger impoundment depth. There was a slight discrepancy noted in the hydrodynamic force occurring at a time of roughly 5.5s (Figure 12) for the lower impoundment depths as the hydrodynamic force began to decrease, this is believed to correspond to the presence of the bore behind the structure. A possible reason for the numerical model's poor estimation of the impact force may be due to the debris propagation errors outlined in the previous section. It was also found that the debris stopping time, length of time from impact to maximum force, was typically double in the numerical model comparing to the experimental test.

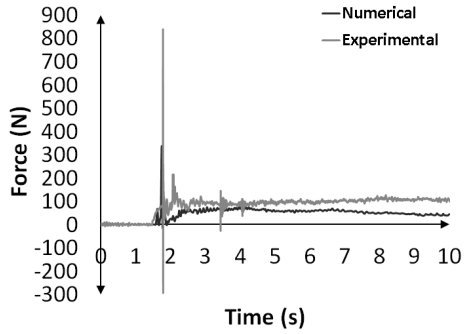

Figure 12. Debris and hydrodynamic impact force comparison for an impoundment depth of 0.55m

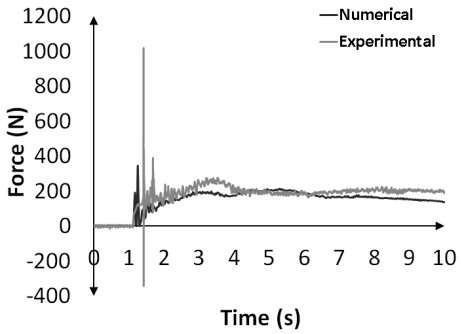

Figure 13. Debris and hydrodynamic impact force comparison for an impoundment depth of 0.85m

Comparison with Analytical Impact Forces

The maximum impact force acting on the structure in the numerical and physical models were compared to the results obtained using prescriptions of FEMA P-55 [2011] and FEMA P-646 [2012], as described in a previous section. This comparison, shown in Figure 14, indicates that FEMA P-646 is better at capturing the high impact forces acting on the structure as seen in the physical model, while the present numerical model and FEMA P-55 significantly underestimate these forces. Improvements for the estimation of the debris impact appear to be necessary in order to properly quantify the debris impact forces acting on structures.

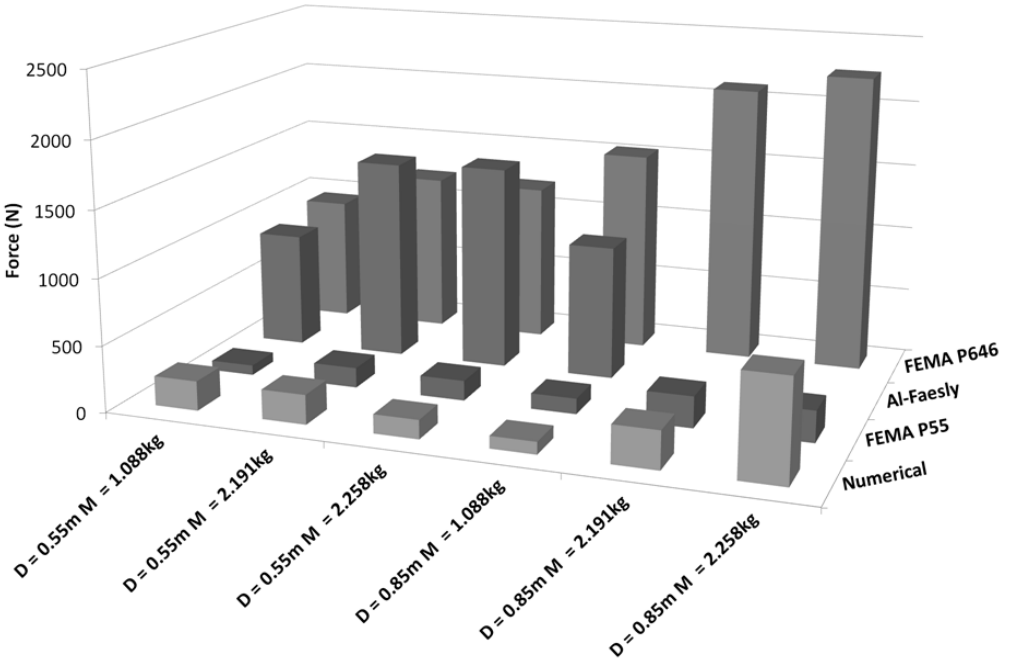

Figure 14. Comparison between physically, numerically, and analytically-calculated debris impact forces on the structure

Debris Propagation through Coastal Forests

This section presents a few of the results of the numerical model used to investigate the attenuation effect of coastal forest. There were four different debris locations tested for this model scenario, with the intent of determining if the initial position of the debris would result in a difference in the runup of the bore and in the debris propagation. This was difficult to determine due to movement from the debris before the arrival of the bore. In one particular case, shown in Figure 15, it can be seen that a direct impact on the coastal forest occurred, resulting in a significantly decreased inland propagation for the debris, whereas in Figure 16, no debris impact occurred during runup.

It was found that the potential debris impact forces on the trees could be larger than the hydrodynamic impact force acting on the trees, indicating a potential risk for tree overturning. However, as shown in Figure 15, numerical results do indicate that a coastal forest has the potential to attenuate tsunami borne debris. However, as seen in Figure 16, a narrow stretch of forest may not be effective in halting the debris propagation as the debris may simply pass through the forest without any impacts. Therefore, it's believed that a larger, denser forest with a staggered tree layout would have the greatest potential to attenuate tsunami-borne debris.

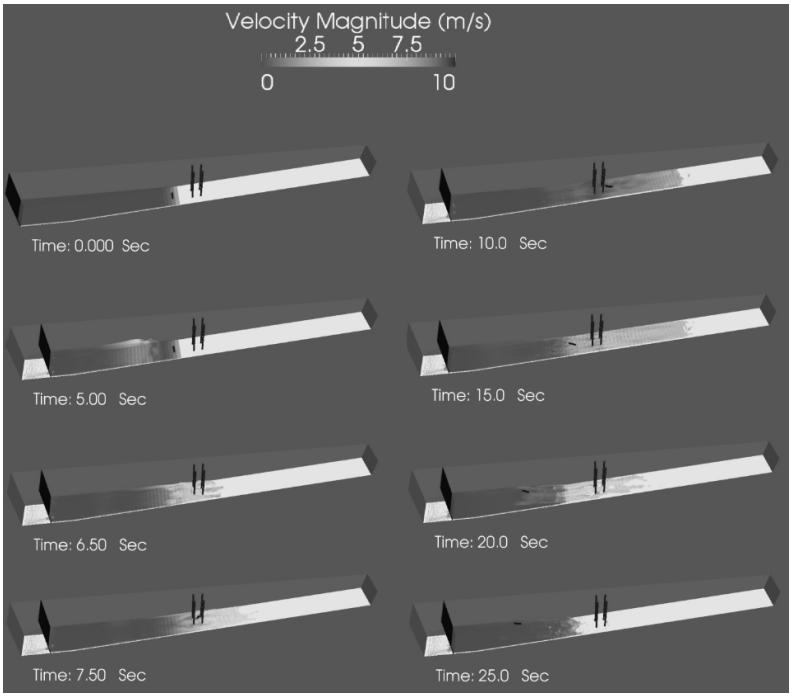

Figure 15. Debris propagation for transversely-placed debris

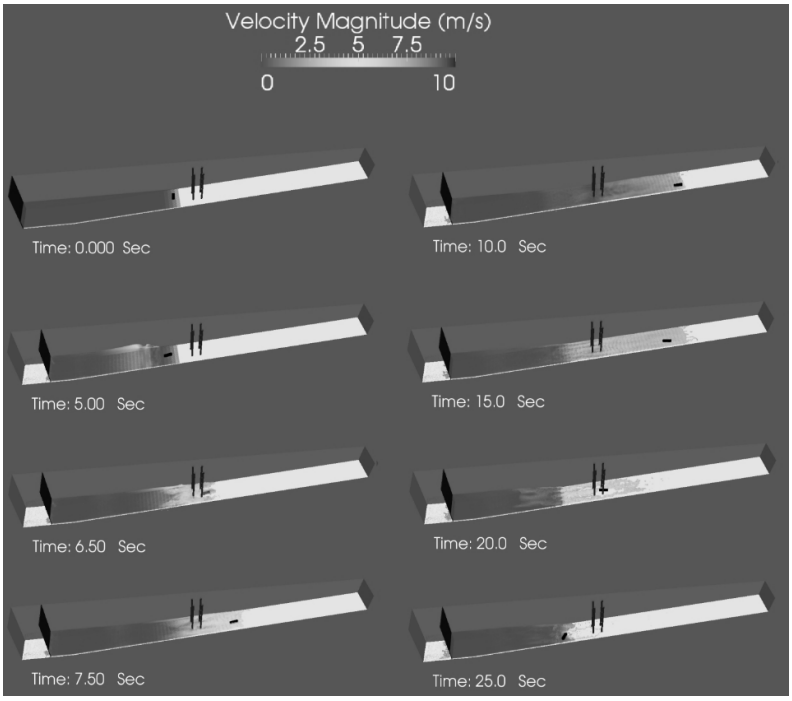

Figure 8. Debris propagation for upright debris

CONCLUSIONS

The purpose of this study was both to examine the suitability of the DualSPHysics SPH model to model debris propagation and debris impacts on a rigid structure, and to also determine the potential of a coastal forest to attenuate the propagation of tsunami-borne debris. The first objective was completed by comparing the numerical results of the model to the physical model completed by Al-Faesly *et al*.

[2013] using various impoundment depths and debris sizes/masses to determine the suitability of the numerical model, while the second objective focused on examining the results of the debris propagation and impacts on a large-scale coastal forest model.

When comparing the results of the physical and numerical model it was found that the water surface elevation in the numerical model was in good agreement with the physical model results except at the front of the structure. This was caused by inaccuracies in modeling of the debris propagation which caused the debris to reach the structure before the bore and block the bore from running up the structure. In addition, it was found that the large impact forces obtained in the physical model could not be replicated by the numerical model. It is hypothesized that these results could be improved by the using of a friction coefficient between the debris and the modeled flume floor as the debris moved very freely. Further improvements could also be made by using a smaller particle-spacing as this would allow the bore to get closer to the debris, and may result in a reduced debris stopping-time which would allow for higher impact forces. When compared to the physical and analytical results, it could be seen that both FEMA P-55 [2011] and the numerical results did not properly estimate the debris impact forces seen in the physical model; however the FEMA P-646 [2012] results were fairly close. This indicates that the use of the FEMA P-55 equation could result in a gross underestimation of the potential impact force on the structure.

When examining the effect of a coastal forest on the tsunami-borne debris propagation it was shown that, depending on the debris mass and flow characteristics, debris impact forces could be larger than the hydrodynamic impact forces. It was also shown that the coastal forest do have the potential to attenuate the propagation of the debris and may be an effective barrier against both the tsunami and the associated debris.

REFERENCES

Al-Faesly, T., I. Nistor, D. Palermo, and A. Cornett. 2013. Experimental Study of Structures Subjected to Hydrodynamic and Debris Impact Forces. *Canadian Society of Civil Engineers.* Montreal.

ASCE. 2010. Minimum Design Loads for Buildings and Other Structures, *ASCE/SEI Standard 7-10*, American Society of Civil Engineers, Reston, Virginia.

Batchelor, G.K. 1967. *An Introduction to Fluid Dynamics.* Cambridge: Cambridge University Press.

Benz, W. 1990. Smoothed Particles Hydrodynamics: a Review. In *Numerical Modeling of Non-Linear Stellar Pulsation: Problem and Prospects*, by de Jager C. Boston: Kluwer Academics.

Crespo, A. J. C., M. Gomez-Gesteira, and R. A. Dalrymple. 2007. Boundary Conditions Generated by Dynamic Particles in SPH Methods. *Computers, Materials and Continua*, 173-184.

Crespo, A. J. C., J. M. Dominguez, A. Barreiro, M. Gomez-Gesteira, and B. D. Rogers. 2011. GPUs, a New Tool of Acceleration in CFD; Efficiency and Reliability on Smoothed Particle Hydrodynamics Method. *PLoS ONE*.

FEMA. 2011. *Coastal Construction Manual.* FEMA P55, Federal Emergency Management Agency.

FEMA. 2012. *Guidelines for Design of Structures for Vertical Evacuation from Tsunamis - Second Edition.* FEMA P646, Federal Emergency Management Agency.

Gingold, R. A., and J. J. Monaghan. 1977. Smoothed Particle Hydrodynamics: Theory and Application to Non-Spherical Stars. *Monthly Notices of the Royal Astronomical Society*, 375-389.

Gomez-Gesteira, M., B. D. Rogers, R. A. Dalrymple, A. J. C. Crespo, and M. Narayanaswamy. 2010. User Guide for the SPHysics Code.

Gomez-Gesteira, M., A. J. C. Crespo, B. D. Rogers, R. A. Dalrymple, J. M. Dominguez, and A. Barreiro. 2012b. SPHysics - Development of a Free-Surface Fluid Solver - Part 2: Efficiency and Test Cases." *Computers and Geoscience*.

Gomez-Gesteira, M., B. D. Rogers, A. J. C. Crespo, R. A. Dalrymple, M. Narayanaswamy, and J. M. Dominguez. 2012a SPHysics - Development of a free-surface fluid solver - Part 1: Theory and Formulations." *Computers and Geosciences*.

Liu, M.B., and G.R. Liu. 2003. *Smoothed Particle Hydrodynamics: A Meshfree Particle Method.* MA, USA: World Scientific Publishing.

Lo, E. Y. M., and S. Shao. 2002. Simulation of Near-Shore Solitary Wave Mechanics by an Incompressible SPH Method."*Applied Ocean Research*, 275-286.

Lucy, L. B. 1977. A Numerical Approach to the Testing of the Fission Hypothesis. *The Astronomical Journal*, 1013-1024.

Monaghan, J. J. 1989. On the Problem of Penetration in Particle Methods. *Journal of Computational Physics*.

Monaghan, J. J. 1994. Simulating Free Surface Flows with SPH. *Journal of Computational Physics*, 399 - 405.

Monaghan, J. J. 2005. Smoothed Particle Hydrodynamics. *Reports on Progress in Physics*, 1703-1759.

St-Germain, Philippe. 2012. *Numerical Modeling of Tsunami-Induced Hydrodynamic Forces on Free-Standing Structures using the SPH Method.* Masters Thesis, Ottawa, Canada: University of Ottawa.

Verlet, L. 1967. Computer "Experiments on Classical Fluids. I. Thermodynamical Properties of Lennard-Jones Molecules." *Physical Review*, Vol. 159, No. 1, 98 - 103.